

# Prediction of Load-bearing Capacity of Composite Cylinders with Impact Damage

Aleksandr Cherniaev<sup>1</sup>, Svetlana Pavlova<sup>2</sup>, Aleksandr Pavlov<sup>2</sup>, Valeriy Komarov<sup>2</sup>

<sup>1</sup>Department of Mechanical, Automotive and Materials Engineering, University of Windsor, 401 Sunset Ave., Windsor N9B 3P4, Canada

<sup>2</sup>Samara University, Moskovskoe Hwy 34, Samara 443086, Russia

## 1 Introduction

Impact damage induced by hailstone impact, tool, or equipment dropping can lead to severe reductions in composite structures' load-carrying capacity. Aerospace companies and manufacturers of other products, in which composite materials are extensively used, spend considerable resources to determine the level of degradation of composite parts' load-bearing capacity that have received impact damage during operation or during assembly, as well as the permissible degree of damage at which the replacement of an expensive structural member is unnecessary. Usually, such assessments are based on the integrated application of experimental destructive and non-destructive methods, which, in turn, also requires considerable financial and time investments. Understandably, the availability of a verified simulation approach capable of predicting the residual load-carrying capacity of composite parts with impact damage would provide significant costs savings and accelerate the decision making when such assessments are required. This preliminary study represents the first steps aimed at developing such a simulation approach using LS-DYNA software and is focused on the load-bearing capacity of damaged composite structural members designed to work primarily under the action of compressive loads.

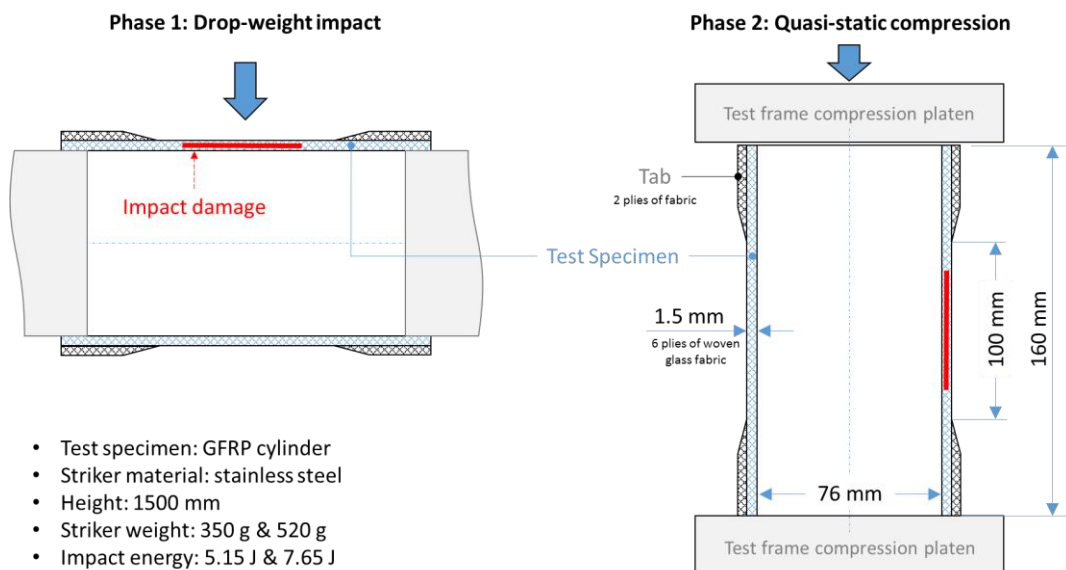


Fig. 1: Experiment schematic

A schematic of two-phase experiments conducted in this study is represented in Fig. 1. In phase 1, the structural components of a cylindrical shape fabricated from composite material were subjected to low-speed impacts by a rigid striker with different impact energies (5.15 J and 7.65 J). In the second phase, damaged composite cylinders were tested in quasi-static compression until failure. Both phases of the physical experiments were then simulated in LS-DYNA and results of numerical predictions were compared with the tests outcomes.

## 2 Materials and manufacturing

A composite material containing approximately 50% of epoxy resin by volume and reinforced by T-26 structural glass fabric was used. The woven fabric had the nominal areal weight of  $285 \pm 12$  g/m<sup>2</sup>, and 11-12 and 6-8 yarns per cm in warp and fill directions, correspondingly. Samples for material characterization were cut from flat panels manufactured using vacuum bagging. Similarly, vacuum bagging was employed in fabricating the composite cylinders. The main stages of the latter process are

illustrated in Fig. 2. After curing, composite parts were trimmed to have the overall length of 160 mm. The warp direction of all fabric layers was oriented at 90 degrees with respect to the cylinder axis.

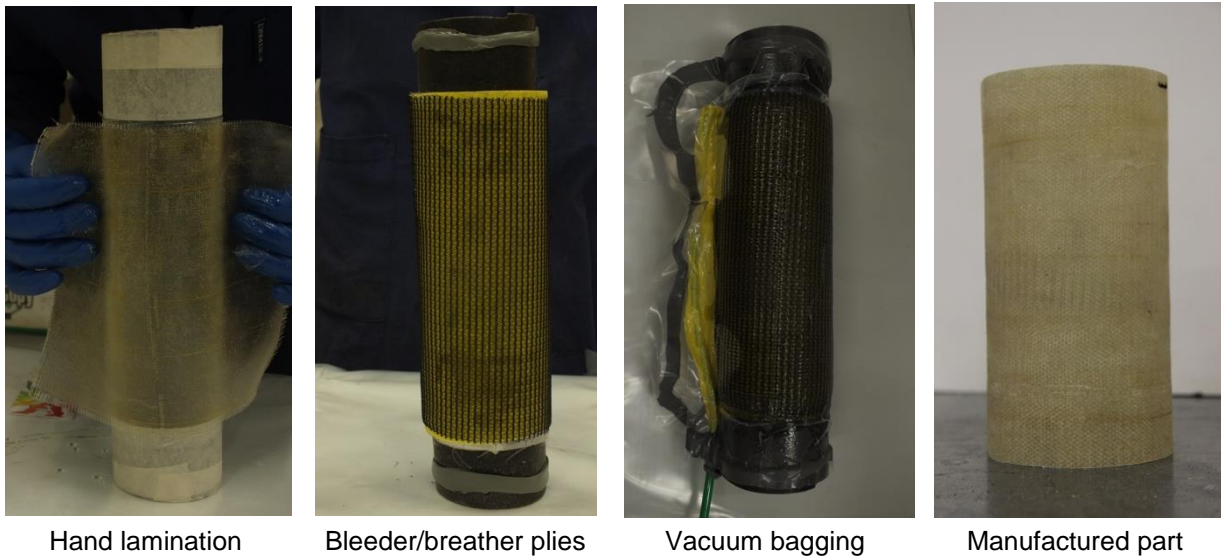


Fig.2: Manufacturing of composite cylinders: main stages

### 3 Experimental methods

All quasi-static experiments, including the material characterization tests and post-impact compression of the composite cylinders, were conducted using an MTS test frame equipped with a 100 kN MTS 661.20F-03 load cell. Crosshead displacement of 2 mm/min was used.

#### 3.1 Material characterization

For material characterization, both intra- and inter-ply properties of the woven glass fabric/epoxy matrix vacuum-bagged composite were experimentally determined. All intra-ply properties tests were conducted according to the corresponding ASTM standards (Fig. 3). Particularly, tensile properties of the composite material along warp and fill directions were determined using the procedure described in the ASTM D 3039 standard [1]. For the shear properties, specimens with a  $\pm 45$  deg. layup were tested in tension according to the ASTM D 3518 test procedure [2]. In these tests, a biaxial extensometer MTS 632.85F-14 was used for strain measurements along and perpendicular to the loading direction. The GFRP composite's compressive properties were obtained according to the ASTM D 3410 standard using the loading and alignment fixtures described in the standard [3].

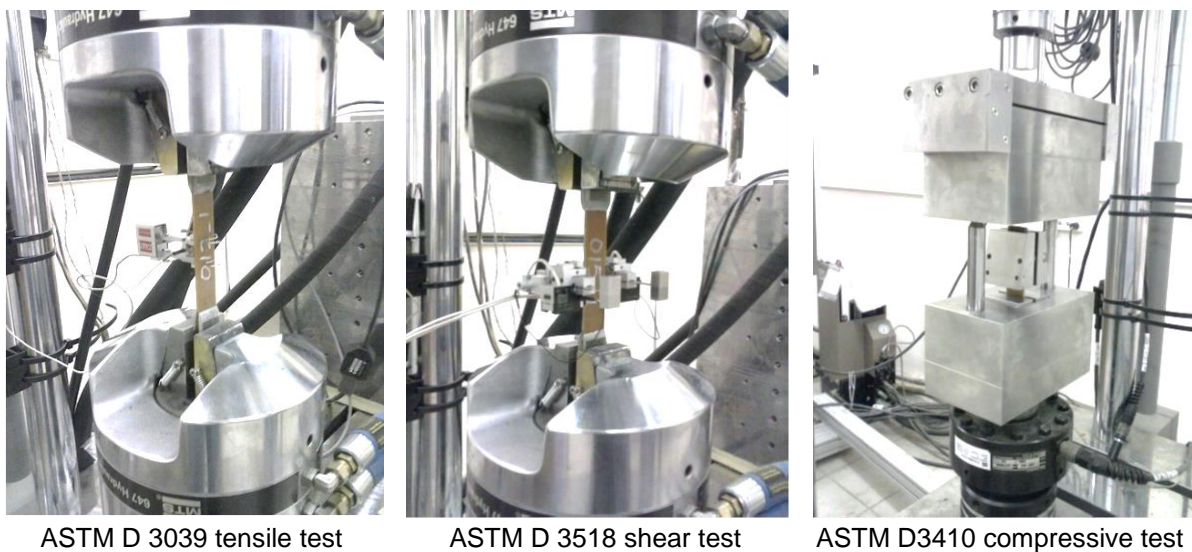


Fig.3: Material characterization: intra-ply properties

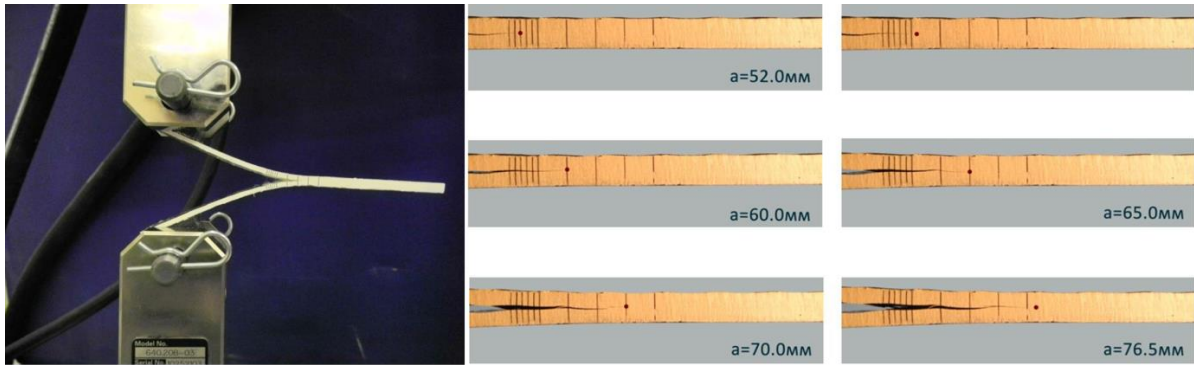


Fig.4: Material characterization: inter-ply properties (mode I interlaminar fracture toughness test)

The composite material's inter-ply properties were characterized using the double-cantilevered beam (DCB) and end-notched flexure (ENF) tests, which allowed for measuring the critical strain energy release rate in mode I ( $G_{Ic}$ ) and mode II ( $G_{IIc}$ ), correspondingly. The former test was conducted following the method described in the ASTM D 5528-01 standard [4], according to which the ends of DCB specimens were subjected to controlled opening displacements while the load and delamination length were recorded (Fig. 4). For the latter test, the method based on subjecting end-notched specimens to three-point bending was employed. A description of this test procedure can be found in [5].

### 3.2 Testing of composite cylinders

A simple drop-weight apparatus, as shown in Fig. 5 (a), was built to induce controlled-energy impact damage to the composite cylinders. As part of this apparatus, a simple mechanism preventing secondary impacts to the cylinders was implemented. This mechanism fixed the stainless-steel striker after bouncing from the surface of the cylinder for the first time. The striker in the fixed position above the composite specimen right after impact is shown in Fig. 5 (b). In all impact tests, strikers were released from a 1.5m height. To induce different levels of damage, strikers of 350g and 520g were used.

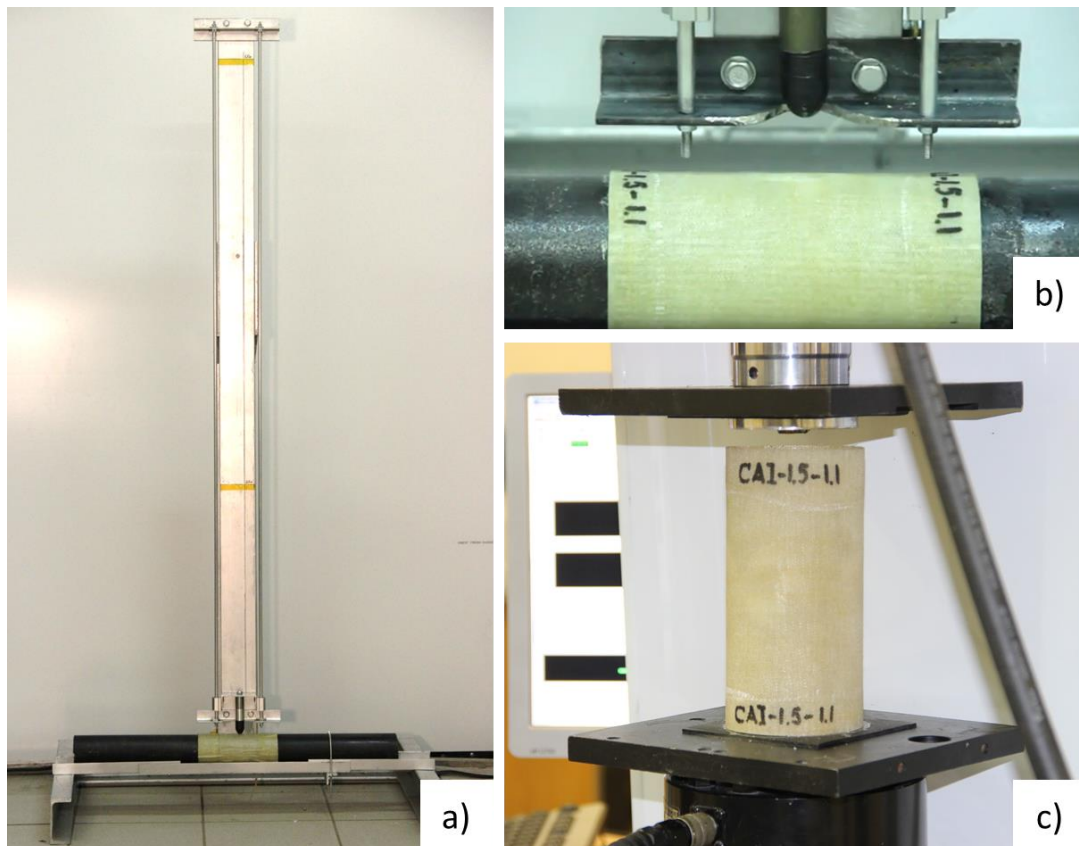


Fig.5: Testing of composite cylinders: impact (a, b) and post-impact compression (c)

Following the impact experiment, damaged composite cylinders were tested until failure under unidirectional compression using the 100 kN MTS test frame. To achieve uniform distribution of the compressive force across the loaded sides of the specimens, thin rubber pads were inserted between the compressive platens of the test frame and the composite cylinders, as can be seen in Fig. 5 (c).

#### 4 Modeling techniques

A finite element model of the two-stage process, involving impact damaging of the composite cylinders and compression after impact, was developed in LS-DYNA. The model's major features are illustrated in Fig. 6. The steel striker in the model was represented by a rigid body with the assigned translational mass (350g or 520g, depending on the modeled impact conditions) and the vertical speed just before impact of 5.425m/s applied using the `*INITIAL_VELOCITY_RIGID_BODY` keyword. The `*CONTACT_ERODING_SURFACE_TO_SURFACE` contact algorithm was used to simulate the striker and the composite cylinder's interactions.

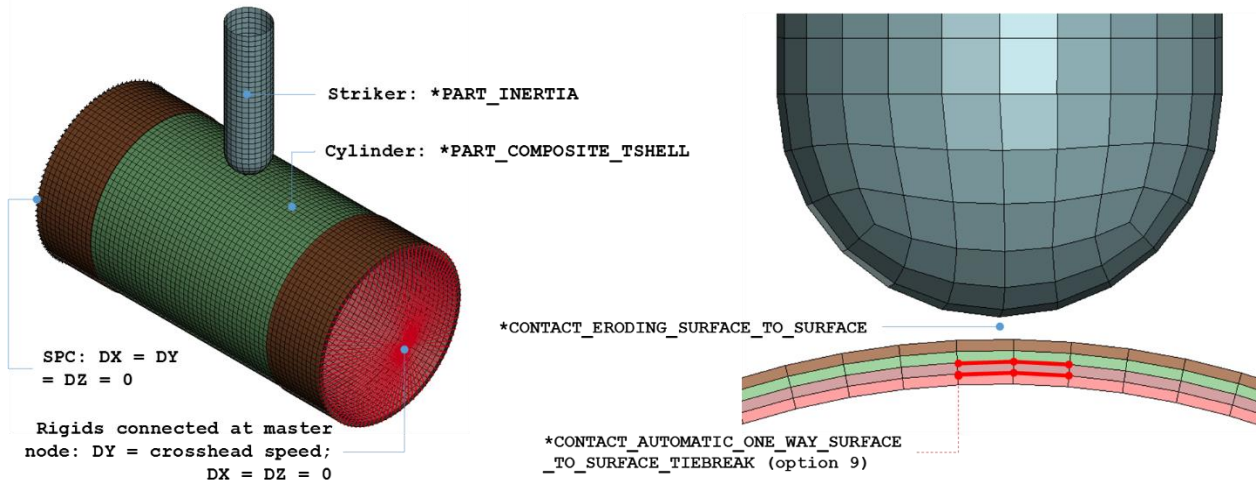


Fig.6: Numerical model

Walls of the cylinders were modeled using three layers of stacked TSHELL elements, each representing two “physical” plies of the woven glass fabric oriented at 90 degrees, i.e. with warp direction being perpendicular to the cylinder’s axis. To represent delamination, the two contact interfaces between the three TSHELL layers were modeled using `*CONTACT_AUTOMATIC_ONE_WAY_SURFACE_TO_SURFACE_TIEBREAK` with `OPTION 9`. This contact algorithm is equivalent to using zero-thickness cohesive zone elements and is based on the fracture model with bilinear traction-separation law, mixed-mode delamination criterion, and damage formulation [6]. This delamination model’s main parameters include normal and shear failure stresses at the interface between the adjacent layers (NFLS and SFLS parameters), mode I and mode II critical strain energy release rates ( $G_{Ic}$  and  $G_{IIc}$ ), and the normal (CN) and tangential ( $CT = CT2CN \times CN$ , where  $CT2CN$  – a coefficient between 0 and 1) stiffness of the material in the interlaminar region. The bilinear law corresponding to a simple case of crack opening (mode I) is exemplified in Fig. 7. A detailed description of the mixed-mode loading treatment in this model can be found in [6]. After satisfaction of the failure criterion ( $\delta > \delta_{ult}$ ), the failed interface (master segment – slave node pair) can only resist compressive forces.

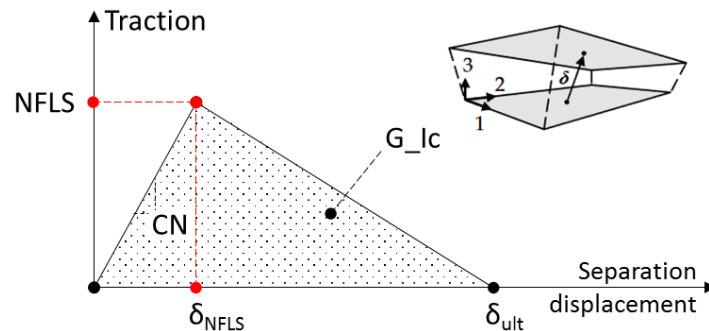


Fig.7: Parameters of the . . . `SURFACE_TO_SURFACE_TIEBREAK` contact with `OPTION 9`

Tabs of the composite cylinders were represented by an additional layer of TSHELL elements and connected to the body of the cylinder using the simple `*CONTACT_TIED_SURFACE_TO_SURFACE` method. Overall evaluation of the contacts between the stacked TSHELL layers was conducted by running implicit eigenvalue analysis and observing the deformation modes corresponding to different eigenvalues. As can be seen in Fig. 8, modeled composite cylinders deform as a single entity, which confirms that all contacts were appropriately engaged.

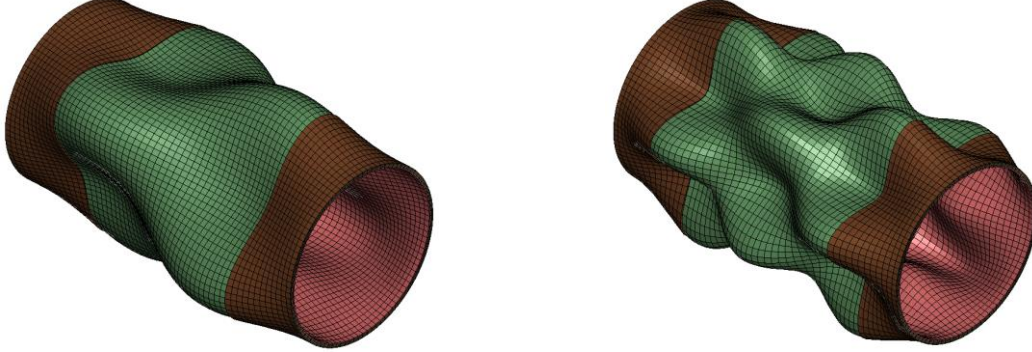


Fig.8: Evaluation of contacts between TSHELL element layers using eigenvalue analysis

`MAT058` or `*MAT_LAMINATED_COMPOSITE_FABRIC` — a damage mechanics-based model, which accounts for both pre- and post-peak softening of composite plies — was used to model the intra-ply behavior of the woven glass fabric-reinforced composite cylinders. Details of this model's implementation can be found in [7]. Depending on the type of failure surface, this model may be used to model composite materials with unidirectional layers, complete laminates, and woven fabrics. In this study, the following set of failure criteria was used to represent the behavior of the fabric-reinforced composite (a.k.a failure surface FS = -1):

$$e_{warp}^2 = \left( \frac{\bar{\sigma}_{11}}{X_{T,C}} \right)^2 - 1, \quad (1)$$

$$e_{fill}^2 = \left( \frac{\bar{\sigma}_{22}}{Y_{T,C}} \right)^2 - 1, \quad (2)$$

$$e_s^2 = \left( \frac{\bar{\tau}_{12}}{S} \right)^2 - 1. \quad (3)$$

Here,  $X_{T,C}$  and  $Y_{T,C}$  represent the material's strength in warp (X) and fill (Y) directions in tension ("T"; used if  $\sigma_{ij} > 0$ ) or compression ("C"; used if  $\sigma_{ij} < 0$ ), and S is the fabric shear strength. It should be noted that the effective stresses ( $\bar{\sigma}_{ij}$ ) in the above expressions are related to the nominal stresses through the damage parameters  $d_{ij}$ , also known as area loss parameters, such that:

$$[\bar{\sigma}] = \begin{bmatrix} \bar{\sigma}_{11} \\ \bar{\sigma}_{22} \\ \bar{\tau}_{12} \end{bmatrix} = \begin{bmatrix} \frac{1}{1-d_{11}} & 0 & 0 \\ 0 & \frac{1}{1-d_{22}} & 0 \\ 0 & 0 & \frac{1}{1-d_{12}} \end{bmatrix} \cdot \begin{bmatrix} \sigma_{11} \\ \sigma_{22} \\ \tau_{12} \end{bmatrix}, \quad (4)$$

where damage evolution with straining is assumed as  $d_{ij} = 1 - \exp \left[ -\frac{1}{m\epsilon} \cdot \left( \frac{\epsilon}{\epsilon_f} \right)^m \right]$ , and m,  $\epsilon$  and  $\epsilon_f$  are the parameters controlling the shape of the stress-strain response, strain, and strain at maximum directional stress, correspondingly. Thus, the components of the constitutive tensor  $C(d)$  can be represented as functions of the damage parameters and the properties of the undamaged layer:

$$C(d) = \frac{1}{D} \begin{bmatrix} (1-d_{11})E_{11} & (1-d_{11})(1-d_{22})\nu_{21}E_{22} & 0 \\ (1-d_{11})(1-d_{22})\nu_{12}E_{11} & (1-d_{22})E_{22} & 0 \\ 0 & 0 & D(1-d_{12})G_{12} \end{bmatrix}, \quad (5)$$

where  $D = 1 - (1-d_{11})(1-d_{22})\nu_{12}\nu_{21} > 0$ .

Such CDM-based formulation provides a smooth increase of damage and, on failure initiation, prevents the instantaneous drop of stresses in the failing element. It should also be noted that the two damage parameters  $d_{11}$  and  $d_{22}$  assume different values for tension ( $d_{11+}$  and  $d_{22+}$ ) and compression ( $d_{11-}$  and  $d_{22-}$ ). Additional non-physical parameters associated with MAT058, as well as reasons for their choice, are described in Table 1.

Table 1: Non-physical parameters for MAT058 (initial pre-calibration values)

Parameter	Meaning	Units	Value	Comment for the chosen initial value
TSIZE	Time step for automatic element deletion.	s	1E-10	Disabled by choosing a very small time step value for element deletion
ERODS	Maximum effective strain for element failure. If lower than zero, the element fails when effective strain calculated from the full strain tensor exceeds ERODS	mm/mm	-2.000	Chosen to be significantly higher than any directional strain at failure initiation.
SLIMT1	Factor to determine the minimum stress limit after stress maximum (fiber tension).	-	0.100	A recommended value [6]
SLIMC1	Factor to determine the minimum stress limit after stress maximum (fiber compression).	-	0.375	A value used in Ref. [8]
SLIMT2	Factor to determine the minimum stress limit after stress maximum (matrix tension).	-	0.100	A recommended value [6]
SLIMC2	Factor to determine the minimum stress limit after stress maximum (matrix compression).	-	0.375	A value used in Ref. [8]
SLIMS	Factor to determine the minimum stress limit after stress maximum (shear).	-	1.000	A recommended value [6]

The post-failure response of composite in **MAT058** is governed by an array of stress limit factors (SLIM\_), which represent the amount of residual strength the composite retains after the element's complete failure. For example, even a completely crushed composite can usually retain some resistance to compressive loading, which can be conveniently represented by stress limit factors in compression along warp (SLIMC1) and fill (SLIMC2) directions. The *initial* values for the stress limit factors presented in Table 1 have been chosen based on the software developer's recommendations provided in Ref. [6] for SLIMT\_ and SLIMS, as well as based on the previous Author's experience of using this material model (see Ref. [8], in which the value of 0.375 for SLIMC1 and SLIMC2 was obtained via calibration with experimental data for the case of axial crushing of CFRP energy absorbers). The idea of stress limit factors is schematically illustrated in Fig. 9, where E11C corresponds to the strain at compressive strength XC and GMS to strain at in-plane shear strength S.

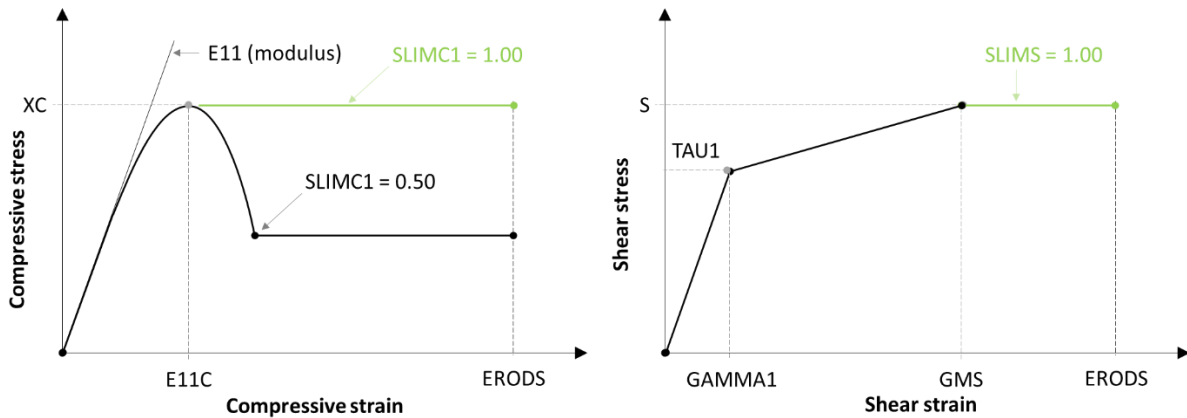


Fig.9: SLIM\_ factors and the bilinear stress-strain diagram for woven fabrics

With failure surface FS=-1, MAT058 provides an option for defining the shear stress-shear strain diagram as a bi-linear curve, which allows for the improved approximation of nonlinear shear behavior of fabric-reinforced materials, which is usually observed experimentally. This model is schematically illustrated in Fig. 9 (right). Parameters TAU1 and GAMMA1 represent, correspondingly, shear stress and shear strain at which behavior of a fabric-reinforced composite becomes nonlinear.

As can be seen in Fig. 6, SPC constraints have been applied on one side of the cylinder while rigid 1D elements connected at a master node have been used to define the boundary conditions on the other side of the cylinder. A displacement imitating the test frame crosshead movement was applied to the master node. The corresponding load curve is shown in Fig. 10. As can be deduced from the figure, no

compressive loading was applied in the first 10ms when the cylinders were subjected to drop-weight impact. Then, the speed of the master node was gradually increased to 20mm/s within the next 10ms and remained at that level for the rest of the simulation. It should be noted that compared to the experiment, somewhat higher speed was used in simulations to reduce the computational time.

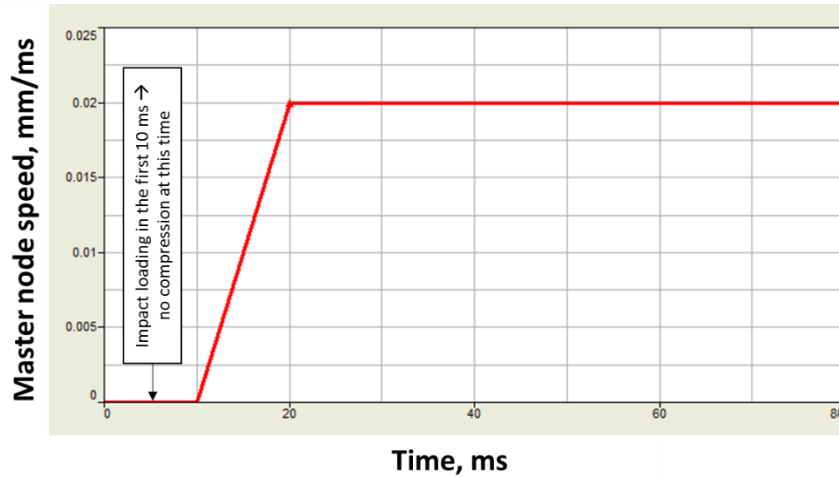


Fig.10: Load curve used in the simulations

## 5 Results and discussion

### 5.1 Material properties

Material properties obtained during the material characterization campaign described in Section 3.1, including the fracture mechanics properties, are summarized in Table 2. The glass fabric composite exhibited a highly nonlinear shear response, as can be seen in Figure 11. Considering this, the MAT058 failure surface FS=-1 was used with the bilinear approximation for the shear stress-shear strain diagram (see Fig. 11).

Table 2: Measured mechanical properties of the T-26/1430 composite

Property	Value	Standard deviation	Test method
Longitudinal Young's modulus (E1), MPa	20800	1600	ASTM D 3039
Transverse Young's modulus (E2), MPa	12200	740	ASTM D 3039
Poisson's ratio ( $\nu_{12}$ )	0.079	n/a	ASTM D 3039
Shear modulus (G12), MPa	2950	53.12	ASTM D 3518
Tensile strength in warp direction (Xt), MPa	397	22.64	ASTM D 3039
Compressive strength in warp direction (Xc), MPa,	153	5.76	ASTM D 3410
Tensile strength in fill direction (Yt), MPa	240	14.59	ASTM D 3039
Compressive strength in fill direction (Yc), MPa	101	5.32	ASTM D 3410
Shear stress at onset of nonlinearity, MPa	25 (see Fig 11)	n/a	ASTM D 3518
Shear stress at 5% shear strain, MPa	33	1.87	ASTM D 3518
Mode I critical strain energy release rate ( $G_{Ic}$ ), kJ/m <sup>2</sup>	0.24	0.02	ASTM D 5528-01
Mode II critical strain energy release rate ( $G_{IIc}$ ), kJ/m <sup>2</sup>	1.96	0.50	End-notched flexure

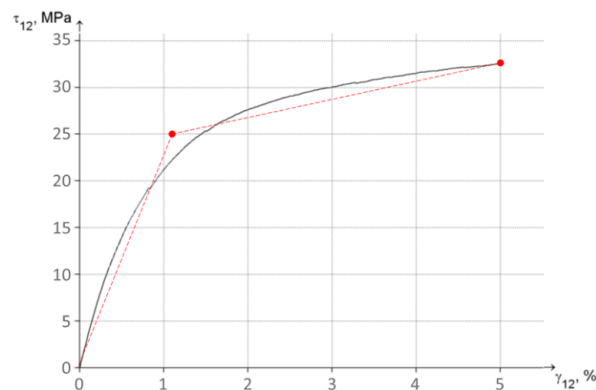


Fig.11: Shear stress – engineering shear strain diagram: experiment and bi-linear idealization for MAT58 woven fabric-specific failure surface FS=-1

Parameters of the delamination model used in this study, as well as the rationale for their choice, are summarized in Table 3.

Table 3: Input data for \*CONTACT\_AUTOMATIC\_ONE\_WAY\_SURFACE\_TO\_SURFACE\_TIEBREAK

Property	Value	Rationale
NFLS, MPa	25.00	NFLS can be bound by the following values: <ul style="list-style-type: none"> <li>• <i>lower bound</i> – the transverse strength of a typical <u>unidirectional</u> GFRP (~40 MPa), which would be a reasonable estimate in the case of interlaminar failure by <i>adhesive mechanism</i> (cracks formed at the interface between the epoxy in the interlaminar resin-rich region and fibers in the layer adjacent to it).</li> <li>• <i>upper bound</i> – the ultimate strength of bulk epoxy resin (~60 MPa), which would be a reasonable estimate in the case of interlaminar failure by <i>cohesive mechanism</i>.</li> </ul> This averages to 50 MPa as an estimate for the max traction parameter. In addition, a <i>scaling factor</i> of 0.5 was used to account for the mesh dependency observed for this delamination model (see the recommendation provided in Ref. [9] for meshes with element sizes between 1 and 3 mm).
SFLS, MPa	14.40	Assumed as SFLS = NFLS / $\sqrt{3}$ (von Mises criterion)
G <sub>lc</sub> , kJ/m <sup>2</sup>	0.24	Measured experimentally, see Table 1
G <sub>llc</sub> , kJ/m <sup>2</sup>	1.96	Measured experimentally, see Table 1
CN, MPa/mm	55,000.00	$CN = E_{epoxy} / \delta_{RRR}$ , where $E_{epoxy}$ is the Young's modulus of epoxy matrix (~1000 MPa) and $\delta_{RRR}$ is the thickness of the interlaminar resin-rich region (typically – within 0.01 and 0.10 mm). Thus, the lower and upper bounds for CN correspond to 10000 MPa/mm and 100000 MPa/mm, accordingly. This averages to 55000 MPa/mm as an estimate for the CN parameter. In addition, the condition for $CN > CN_{min}$ must be ensured (see Ref. [6]), where $CN_{min} = (1/2) * (NFLS^2) / (G_{lc})$ . This condition is satisfied for the listed set of parameters of the delamination model.
CT2CN, –	0.37	$CT2CN = CT / CN = G_{epoxy} / E_{epoxy} = 1 / 2 * (1 + \nu_{epoxy})$ , where $G_{epoxy}$ and $\nu_{epoxy}$ are the shear modulus and the Poisson's ratio (~0.35) of epoxy resin, correspondingly.

## 5.2 Impact damage of composite cylinders

Predicted deformations of the composite shell under the two different impact conditions are compared in Fig. 12. No perforation of the composite by the strikers was predicted, which correlates with the outcomes of the physical experiments.

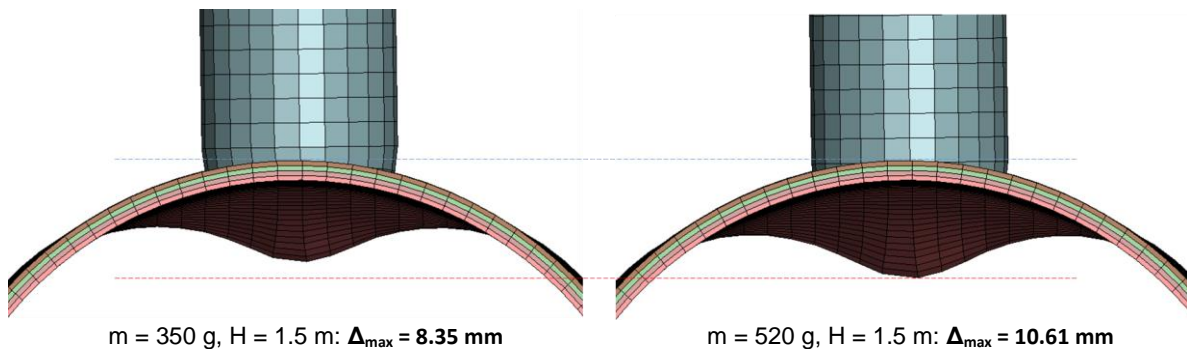


Fig.12: The maximum deflection of the composite cylinders during the impact

Predicted impact damage, as well as the impact damage visible on the tested specimens, is illustrated in figures 13-14. It should be noted that, as discussed in the next section, using the “initial” values of the stress limit factors (SLIM<sub>l</sub>) of MAT058 model resulted in significant under-prediction of the composite cylinders’ load-bearing capacity. Therefore, higher values were used in the second round of simulations (in particular, both SLIMC coefficients were increased from 0.375 to 0.600), and results shown in Figures 13-15 correspond to these increased values. In addition, in Figures 13-14, damage is shown for the outer ply only while delamination is only shown for the interface between the outer and middle plies. In more detail, delamination predicted for the two impact conditions is illustrated in Fig. 15. As can be deduced from Figures 13-14, visible damage mainly corresponds to matrix cracking produced by shear stress during impact.

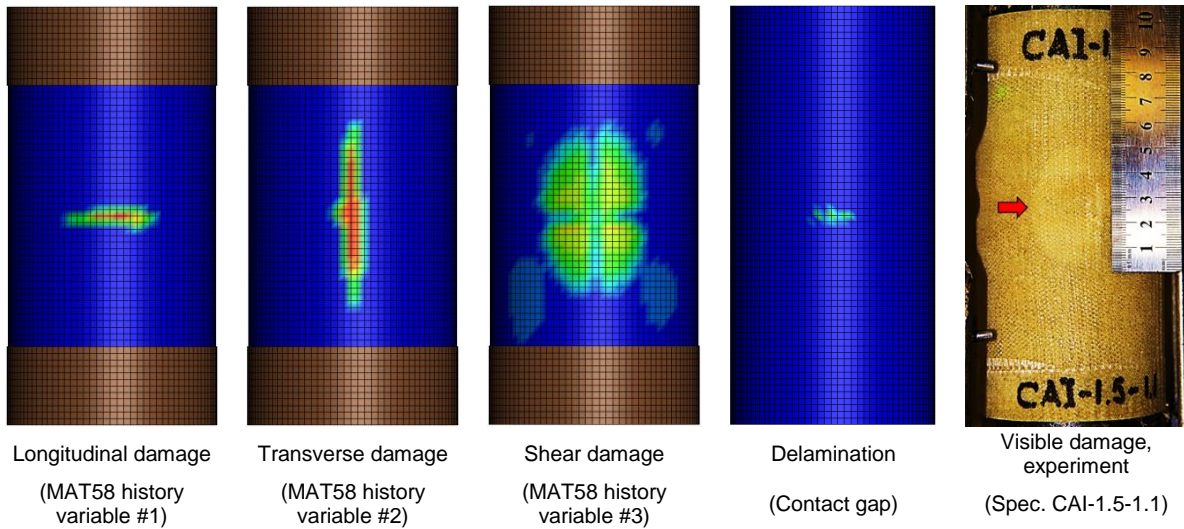


Fig. 13: Composite cylinder hit by 0.35 kg striker released from 1.5 m: comparison of simulation (color scheme: blue – no damage, red – fully damaged) and the physical experiment

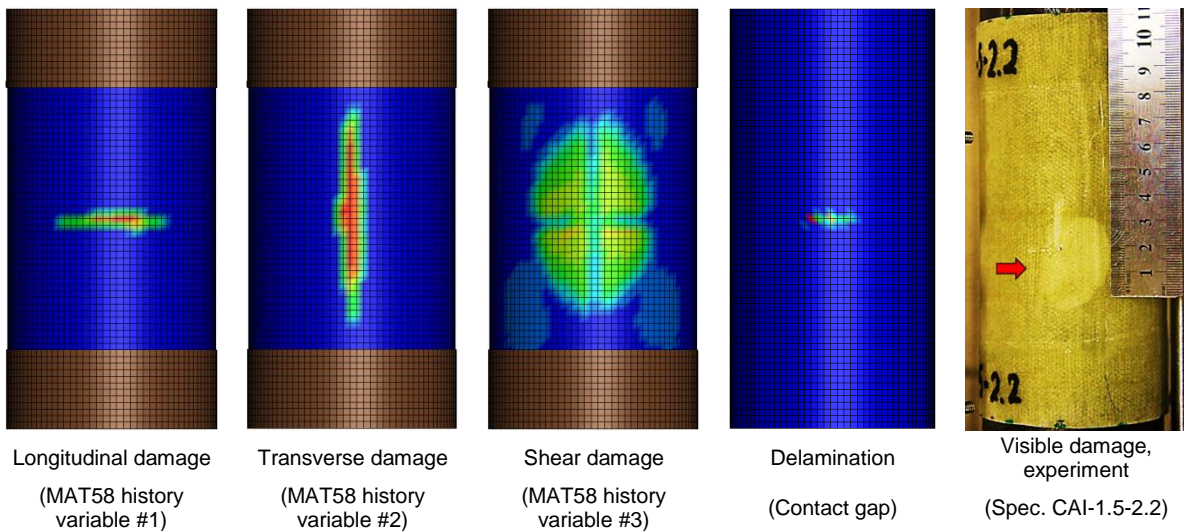


Fig. 14: Composite cylinder hit by 0.52 kg striker released from 1.5 m: comparison of simulation (color scheme: blue – no damage, red – fully damaged) and the physical experiment

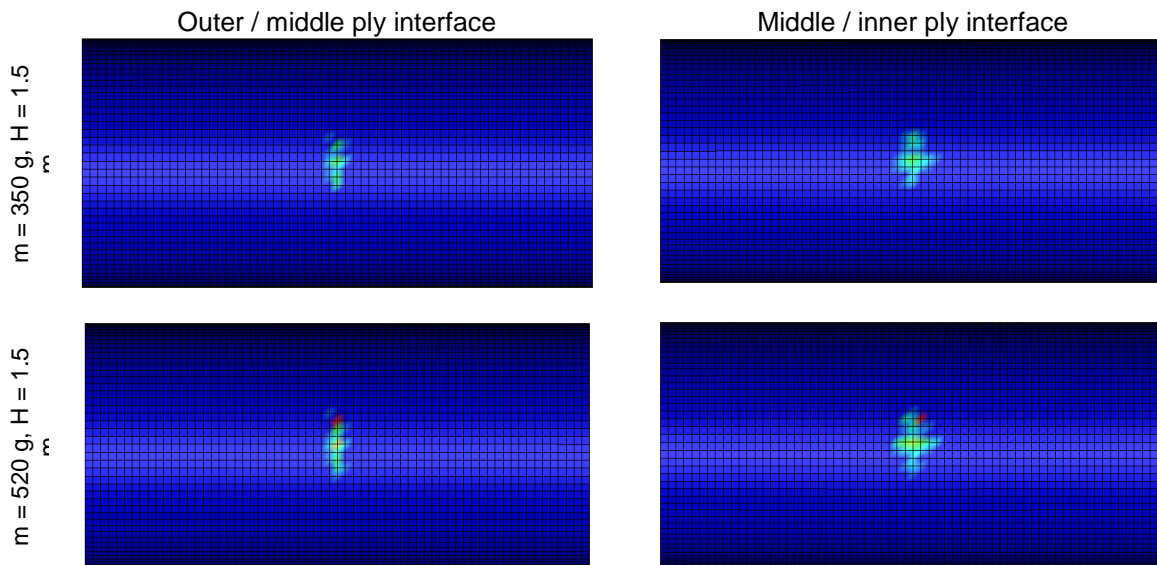


Fig. 15: Predicted delamination (color scheme: blue – no damage, red – fully damaged)

### 5.3 The load-bearing capacity of composite cylinders

Compressive force-displacement diagrams for the two experimentally tested pre-damaged composite cylinders are shown in Fig. 16. The initial nonlinearity of the compressive response visible in the figure should be attributed to the deformation of the rubber pads inserted between the compressive platens and the cylinders to provide a uniform load distribution (see Section 3.2). Maximal compressive force endured by the composite cylinder impacted by a 350g striker corresponded to approx. 30 kN while the cylinder impacted by a 520g weight could support the force of approximately 28.5 kN before failure.

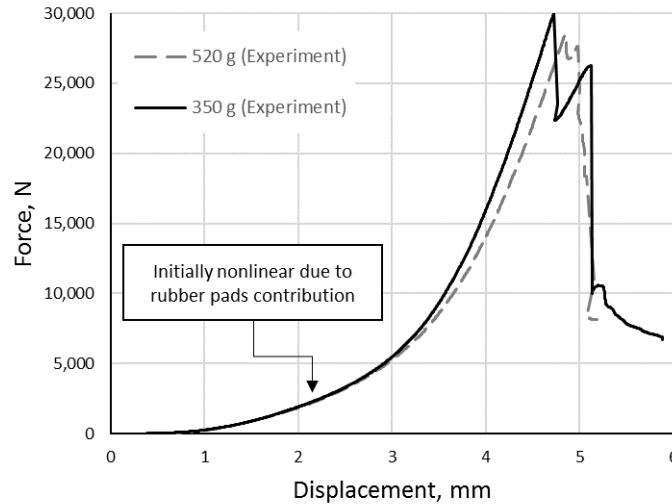


Fig. 16: Force-displacement diagram from the compression after impact experiments

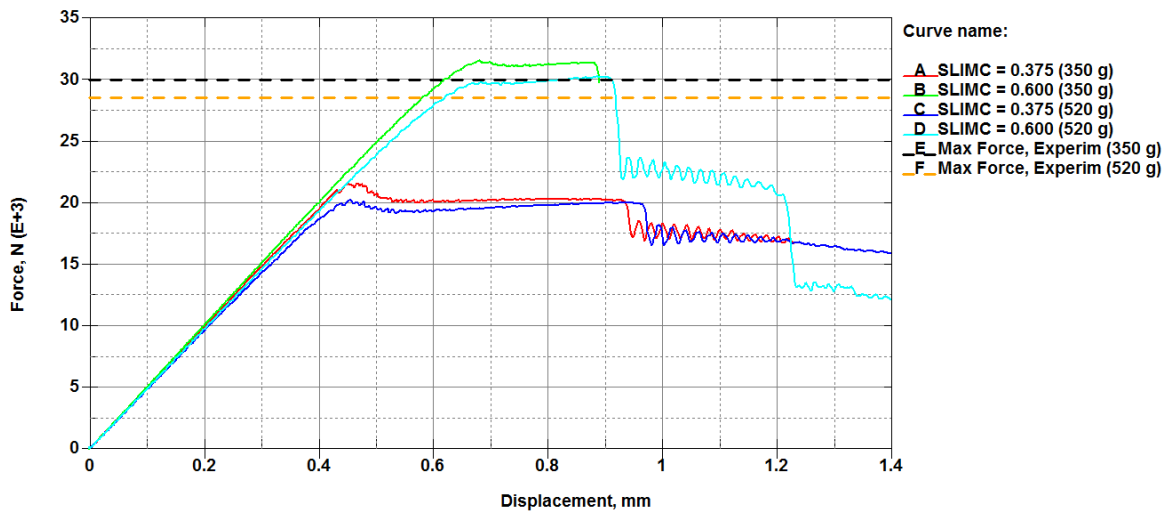


Fig. 17: Simulations of the compression after impact tests with different values of SLIMC factors

Force-displacement diagrams obtained from the first set of simulations demonstrated some under-prediction (~30%) of the composite cylinders' load-bearing capacity when compared with the test results. These diagrams are shown in dark-blue and red in Fig. 17. It can also be seen that for both impact conditions, the predicted response of the cylinders was almost identical. Based on the MAT058 formulation (see Section 4), as well as the previous experience of using this material model [8], it was realized that this behavior may be attributed to the choice of stress limit factors — nonphysical parameters of MAT058 governing the post-failure response of the material. To investigate the SLIM factors' influence, an additional set of simulations was conducted. In these simulations, increased values for compressive limit factors were implemented: SLIMC1 = SLIMC2 = 0.6. The corresponding force-displacement curves are shown in green and light-blue in Fig. 17. They represent a dramatic change of the predicted cylinders' response to compressive loading, only slightly (~5%) over-predicting the experimentally observed load-bearing capacities of the damaged composite parts. It should be noted

however that no rationale exists for determining the optimal SLIMC values and the only method known to the authors would be calibrating using experimental data through a trial-and-error approach.

Figure 18 demonstrates the failure modes of the tested composite cylinders, as well as the predictions obtained using LS-DYNA. Contour plots in this figure correspond to the effective strain (history variable#15 of **MAT058**).

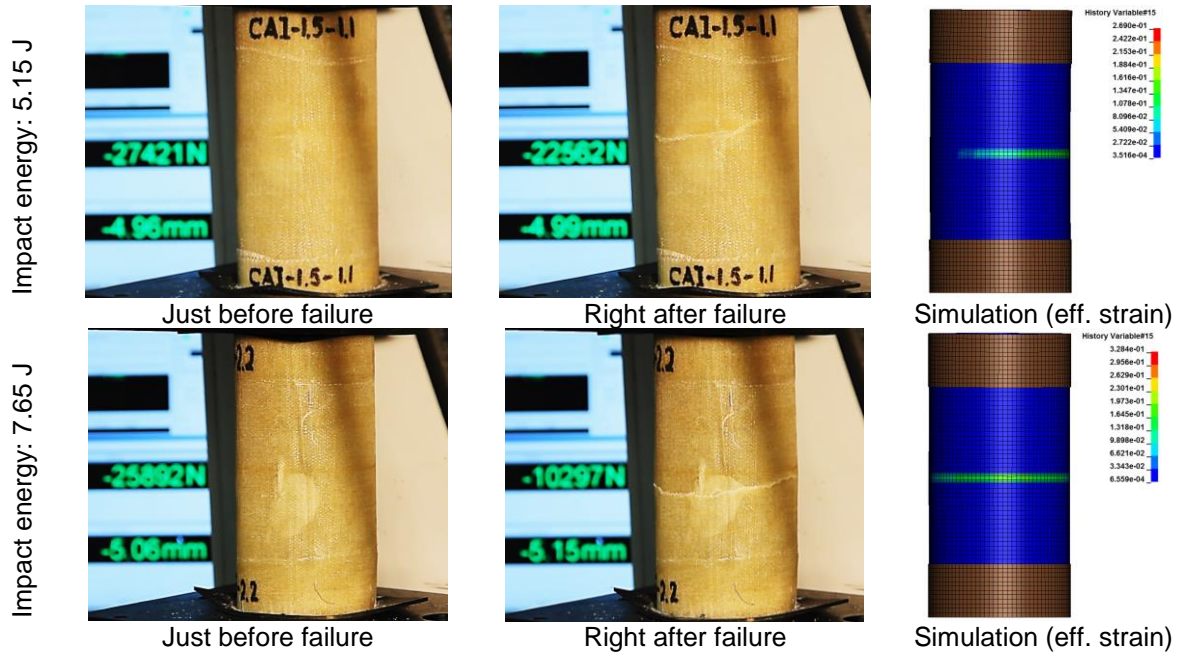


Fig.18: Failure modes of the compressed composite cylinders with impact damage: experiment and simulation

## 6 Summary

In this preliminary study, the capability of LS-DYNA to predict the load-bearing capacity of composite parts with impact damage was investigated. Composite cylinders with impact damage were tested in compression until failure and the same scenario was modeled in LS-DYNA. In the stacked TShell model, **MAT058** (**\*MAT\_LAMINATED\_COMPOSITE\_FABRIC**) and **\*CONTACT\_AUTOMATIC\_ONE\_WAY\_SURFACE\_TO\_SURFACE\_TIEBREAK** with **OPTION 9** were employed for simulating intralaminar and interlaminar damage, correspondingly. The investigation identified stress limit factors SLIMC of **MAT058** as parameters significantly influencing the fidelity of the model. To further advance the predictive capabilities of the model, it is important to develop a formal procedure for the rational choice of these parameters' values. Other important directions for future studies include investigating the developed model's mesh sensitivity and the influence of the delamination model's parameters (NFLS, SFLS, CN, CT) on the predicted load-bearing capacity of composite parts with impact damage.

## 7 Literature

- [1] ASTM Test Method D3039/D3039M-17, Test Method for Tensile Properties of Polymer Matrix Composite Materials, ASTM International, 2017.
- [2] ASTM Test Method D3518/D3518M-13, Standard Test Method for In-Plane Shear Response of Polymer Matrix Composite Materials by Tensile Test of a  $\pm 45^\circ$  Laminate, ASTM International, 2013.
- [3] ASTM Test Method D3410/D3410M-16, Standard Test Method for Compressive Properties of Polymer Matrix Composite Materials with Unsupported Gage Section by Shear Loading, ASTM International, 2016.
- [4] ASTM Test Method D5528-13, Standard Test Method for Mode I Interlaminar Fracture Toughness of Unidirectional Fiber-Reinforced Polymer Matrix Composites, ASTM International, 2013
- [5] Carlsson L.A., Adams D.F., Pipes R.B.: "Experimental Characterization of Advanced Composite Materials", 4th ed., CRC Press, 2014.

- [6] LS-DYNA, ® Keyword user's manual, Volume II: material models, Livermore Software Technology Corporation (LSTC), 2013.
- [7] Schweizerhof K., Weimar K., Münz T., Rottner T.: "Crashworthiness Analysis with Enhanced Composite Material Models in LS-DYNA - Merits and Limits", LS-DYNA Conference, Detroit, Michigan, 1998.
- [8] Cherniaev A., Butcher C., Montesano J.: "Predicting the axial crush response of CFRP tubes using three damage-based constitutive models", Thin-Walled Structures, Volume 129, 2018, pp. 349-364.
- [9] Graf T., Haufe A., Andrade F.: "Adhesives modeling with LS-DYNA: Recent developments and future work", Nordic LS-DYNA Forum, 2014.  
URL: [https://www.dynamore.se/en/resources/papers/2014-nordic-ls-dyna-forum-2013-presentations/adhesives-modeling-with-ls-dyna-recent-developments-and-future-work-1/at\\_download/file](https://www.dynamore.se/en/resources/papers/2014-nordic-ls-dyna-forum-2013-presentations/adhesives-modeling-with-ls-dyna-recent-developments-and-future-work-1/at_download/file) (Accessed: May 7, 2019)